

Electronic and magnetic properties of the RuX_3 ($\text{X}=\text{Cl}, \text{Br}, \text{I}$) family: Two siblings — and a cousin?

David A. S. Kaib,^{1,*} Kira Riedl,^{1,†} Aleksandar Razpopov,¹ Ying Li,² Steffen Backes,³ Igor Mazin,⁴ and Roser Valenti^{1,‡}

¹*Institut für Theoretische Physik, Goethe-Universität, 60438 Frankfurt am Main, Germany*

²*Department of Applied Physics and MOE Key Laboratory for Nonequilibrium Synthesis and Modulation of Condensed Matter, School of Physics, Xi'an Jiaotong University, Xi'an 710049, China*

³*CPHT, CNRS, Ecole Polytechnique, Institut Polytechnique de Paris, Route de Saclay, 91128 Palaiseau, France*

⁴*Department of Physics and Astronomy, George Mason University, Fairfax, Virginia 22030, United States*

(Dated: March 24, 2022)

Motivated by recent reports of metallic behavior in the newly synthesized RuI_3 , in contrast to the Mott-insulating nature of the actively discussed $\alpha\text{-RuCl}_3$, as well as RuBr_3 , we present a detailed comparative analysis of the electronic and magnetic properties of this family of trihalides. Using a combination of first-principles calculations and effective-model considerations, we conclude that RuI_3 , similarly to the other two members, is most probably on the verge of a Mott insulator, but with much smaller magnetic moments and a strong magnetic frustration. We predict the ideal pristine crystal of RuI_3 to have a nearly vanishing conventional nearest-neighbor Heisenberg interaction and to be a quantum spin liquid candidate of possibly different kind than the Kitaev spin liquid. In order to understand the apparent contradiction to the reported resistivity ρ , we analyze the experimental evidence for all three compounds and propose a scenario for the observed metallicity in existing samples of RuI_3 . Furthermore, for the Mott insulator RuBr_3 we obtain a magnetic Hamiltonian of a similar form to that in the much discussed $\alpha\text{-RuCl}_3$ and show that this Hamiltonian is in agreement with experimental evidence in RuBr_3 .

INTRODUCTION

RuI_3 and RuBr_3 are new additions to the RuX_3 family ($\text{X}=\text{Cl}, \text{Br}, \text{I}$) of layered Ru-based trihalides (Fig. 1a). The first member, $\alpha\text{-RuCl}_3$ (in the following “ RuCl_3 ”) has attracted considerable attention in recent years as a candidate material for the Kitaev honeycomb model [1]. RuCl_3 is a spin-orbit assisted Mott insulator whose magnetic low-energy degrees of freedom can be described in terms of $j_{\text{eff}} = 1/2$ moments that interact through strongly anisotropic exchange [2–4]. While the material enters a so-called zigzag antiferromagnetic order (Fig. 1b) at low temperatures $T_N \approx 7\text{ K}$ [5–7], various experiments at finite temperature [8–11] or at finite magnetic field [5, 12–15] have been interpreted as hallmarks of Kitaev physics, a subject which is presently under intensive debate [16–21].

Recently, a sister compound with a heavier halogen, $\text{X} = \text{Br}$, was synthesized [22]. Analogous to RuCl_3 , it is insulating and shows zigzag magnetic order, albeit with higher Néel temperature $T_N = 34\text{ K}$ [22]. In contrast to RuCl_3 , the authors of Ref. 22 reported a Weiss constant with dominant *antiferromagnetic* interactions and a direction of the zigzag ordered moment different from RuCl_3 , and argued that this deviation suggests a closer proximity to the pure Kitaev model.

To complete the RuX_3 family, two independent groups have now synthesized RuI_3 with the even heavier halogen iodine

[23, 24]. In contrast to the two “sibling” compounds, a quasi-metallic behavior was observed in RuI_3 , questioning the description in terms of localized $j_{\text{eff}} = \frac{1}{2}$ -moments. Even though the dc resistivities measured in RuI_3 are orders of magnitude smaller than those of RuCl_3 or RuBr_3 , the reported values of 10^{-3} to $10^{-2}\ \Omega\text{ cm}$ [24] are uncharacteristically large for metals or even typical *bad metals* [25], and practically temperature-independent. While neither of the groups found clear signatures of magnetic ordering [23, 24], they reported different behaviors of the magnetic susceptibility, which is either found to be temperature-independent [24], or with a strong upturn at low temperatures [23], suggesting that sample quality plays a crucial role.

In order to understand the apparently distinct behavior of this family of trihalide materials, in this work we analyze the available experimental data and perform a detailed comparative study of the electronic and magnetic properties of the systems via first-principles calculations and extracted low-energy models. We find that: (i) The behavior of RuI_3 is not that far from RuCl_3 and RuBr_3 and the variations across the series are more quantitative than qualitative. (ii) Pristine samples of RuI_3 should be insulating with highly anisotropic magnetic exchange and nearly vanishing conventional Heisenberg interaction. We argue that the reported metallic behavior in RuI_3 could have its origin in sample quality. (iii) The magnetism in the Mott insulator RuBr_3 has predominantly ferromagnetic interactions, in contrast to what is suggested by the Curie-Weiss analysis of Ref. [22]. We show that such interactions are consistent with experiment when taking into account spin-orbit coupling effects in the Curie-Weiss behavior.

* kaib@itp.uni-frankfurt.de

† riedl@itp.uni-frankfurt.de

‡ valenti@itp.uni-frankfurt.de

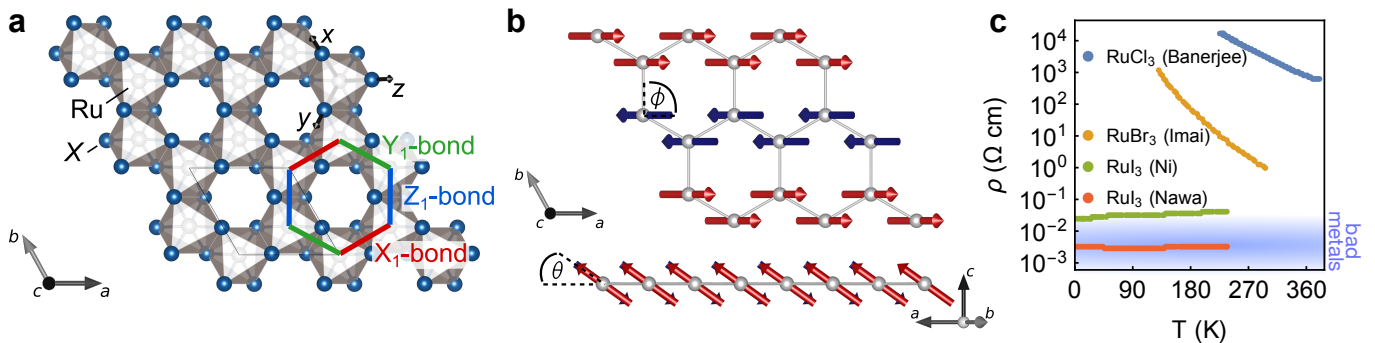


FIG. 1. **RuX_3 ($X=\text{Cl, Br, I}$) crystal structure, magnetic structure and resistivity.** **a** Honeycomb layer in the RuX_3 ($X=\text{Cl, Br, I}$) trihalides with bond definitions, cubic axes (xyz) and crystallographic axes (abc) in the $R\bar{3}$ structure, **b** zigzag magnetic order in a honeycomb layer from two perspectives, with definitions of in-plane-angle ϕ and out-of-plane-angle θ . **c** Comparison of experimental dc resistivities as a function of temperature. Data was extracted from plots in the following references and labelled by respective first-author names: RuCl_3 (Banerjee [7]), RuBr_3 (Imai [22]), Ru_3 (Ni [23], Nawa [24]). The shaded background depicts a typical range of resistivity for bad metals [25].

Our study provides *ab-initio*-derived model parameters and magnetic Hamiltonians for the whole RuX_3 family, that will be useful for future theoretical studies of these systems. As a matter of fact, we show that the microscopic mechanism for the magnetic exchange in RuBr_3 and RuI_3 significantly deviates from the canonically assumed form for the spin-orbit coupling (SOC) [2–4] due to competing SOC contributions from ligands and ruthenium.

RESULTS AND DISCUSSION

Comparative analysis of experiments

In the following, we analyze the reported electrical resistivity, specific heat and magnetic susceptibility data for RuX_3 ($X=\text{Cl, Br, I}$) [7, 22–24, 26].

In Fig. 1c we summarize the temperature dependence of the experimental resistivity data in all three compounds.

In RuI_3 , the resistivity has a weak [23] or almost no [24] temperature dependence (Fig. 1c). Traditionally, metals are classified as materials where the resistivity ρ increases with temperature, distinguishing *conventional metals* (e.g., Cu) as those where in clean samples at temperatures roughly 300 to 600 K, $\rho \sim 10^{-6} \Omega \cdot \text{cm}$ to $\sim 10^{-5} \Omega \cdot \text{cm}$, and *bad metals* as those with resistivities of $\sim 1 - 10 \text{ m}\Omega \cdot \text{cm}$. This range is shown as a background shading in Fig. 1c. The reported resistivities for RuI_3 ($\rho \sim 40 \text{ m}\Omega \cdot \text{cm}$ [23]) and $\rho \sim 4 \text{ m}\Omega \cdot \text{cm}$ [24]) are high even for bad metals, surpassing the Ioffe-Regel limit by more than an order of magnitude. Even more relevant, the *lower-resistivity* set of data [24] shows no discernible temperature dependence at all, while the data in Ref. 23 show a very weak positive derivative $d\rho/dT$, but the absolute value is above anything traditionally considered metallic.

Seemingly, as also pointed out in Ref. 23, electron transport in existing RuI_3 samples may be contaminated by grain

boundaries. One possibility to interpret the measurements is that the pristine material is metallic, but insulating grain boundaries prevent percolation. Then, the in-grain resistivity can be neglected and what is measured is the resistivity of the insulating grain boundaries. In that case, however, thermal activation of carriers in the boundaries should give a positive temperature gradient of the resistivity, which is not observed. The opposite scenario would be of an insulating behavior in the bulk and (possibly bad) metallic one between the grains. In that case, the large resistivity reflects the small relative volume of metallic boundaries, where the transport is dominated by the residual resistivity. This scenario is compatible with the observations. Apart from grain boundaries contaminating resistivity measurements, disorder (in form of vacancies, stacking faults, etc. [23, 24]) could promote the bulk metallic phase over the Mott-insulating one, as has been shown for example for the Mott insulator $\kappa\text{-(BEDT-TTF)}_2\text{Cu}[\text{N}(\text{CN})_2\text{Cl}]$ [27]. Indeed, in our first-principles calculations discussed below, we find the ideal RuI_3 to already be quite close to a Mott-metal transition.

Turning to the sibling compounds RuCl_3 and RuBr_3 , the resistivity (Fig. 1c) decreases with temperature, as expected for Mott insulators, and both systems show an approximate exponential activation gap behavior, $E_{g,\text{eff}}(T) = -k_B T^2 (d \ln \rho / dT)$, although with a significant blue-shift of the gap with increasing temperatures (see Suppl. Information for analysis of RuCl_3 and RuBr_3 resistivity).

Considering specific heat data in the compounds, the specific heat for RuCl_3 displays a well-defined peak at $T_N \approx 7 \text{ K}$ denoting the onset of the zigzag order, while the onset of long-range magnetic order in RuBr_3 is observed by a kink at $T_N = 34 \text{ K}$ [22]. None of this is observed for RuI_3 [23, 24]. In Table I we summarize specific heat parameters reported experimentally [22–24, 28], where γ (β) is the T -linear (T^3)

Sample	γ	β	T_D	$T_D M_{\text{RuX}_3}^{1/2}$
RuCl ₃ * (Tanaka [28])		1.22	185	1
RuBr ₃ (Imai [22])		1.93	159	1.21
RuI ₃ (Ni [23])	29.3	4.72	118	1.07
RuI ₃ (Nawa [24])	17.7	3.66	129	1.17

TABLE I. **Overview of reported specific heat parameters.** γ (β) is the coefficient of the T -linear (T^3) contribution and given in units of $\text{mJ}\cdot\text{K}^{-2}\cdot\text{mol}^{-1}$ ($\text{mJ}\cdot\text{K}^{-4}\cdot\text{mol}^{-1}$). Debye temperature $T_D = \left(\frac{12\pi^4 NR}{5\beta}\right)^{1/3}$ is given in Kelvin and $T_D M_{\text{RuX}_3}^{1/2}$ as a ratio to the value for RuCl₃ (first row), where M_{RuX_3} is the harmonic average of the RuX₃ mass. (*) Note that the values given for RuCl₃ correspond to the asymptotic field-polarized limit extracted by Tanaka *et al.* [28], as elsewhere at zero field the low-temperature specific heat behavior is dominated by vicinity to the Néel temperature of RuCl₃, causing large magnetic contributions to β .

contribution to $C(T)$.

In RuI₃, the T -linear contribution, even though contaminated by an extrinsic raise at small temperatures in Ref. [23] attributed to the nuclear quadrupole moment of Ru, yields $\gamma \sim 15 - 30 \text{ mJ}\cdot\text{K}^{-2}\cdot\text{mol}^{-1}$ [23, 24]. From our electronic structure calculations of RuI₃ shown below, we find that the unrenormalized metallic (*i.e.*, nonmagnetic, not U -corrected) density of states corresponds to $\gamma_0 \approx 3 \text{ mJ}\cdot\text{K}^{-3}\cdot\text{mol}^{-1}$, suggesting a mass renormalization (if this γ is intrinsic) of a factor of 7–12. In the scenario where the metallic grain boundaries take up a sizeable fraction of the sample volume, this renormalization shall be even stronger, encroaching into the heavy fermions domain. This suggests that the origin of the anomalously large residual heat capacity may not be related to intrinsic metallicity. It is worth noting that the T^3 term β of $C(T)$, on the other hand, is rather reasonable for the three systems and scales roughly as the harmonic average M_{RuX_3} of the atomic masses (last column in Table I).

We now turn our attention to magnetic susceptibility measurements. Figure 2a summarize the powder-averaged measured magnetic susceptibilities $\chi(T)$ as reported in Refs. [22–24, 29]. At low temperatures the RuCl₃ data [29] shows a clear signature of a transition to the ordered magnetic phase at 7 K. For RuBr₃, the Néel transition $T_N \approx 34 \text{ K}$ is less apparent from the susceptibility, but the maximum in $d\chi/dT$ is consistent with the distinct transition seen in NMR relaxation measurements [22]. The experimental report on powder samples of RuBr₃ utilized a standard Curie-Weiss (CW) fit, yielding an average Curie-Weiss temperature $\Theta_{\text{std}}^{\text{avg}} = -58 \text{ K}$ [22], indicating predominantly AFM interactions. However, as we have recently shown [30], the Weiss constants obtained with such a standard CW fit may not anymore reflect the intrinsic exchange couplings in the case of significant SOC in the material, as it is the case for the Ru-based trihalides. With SOC, temperature-

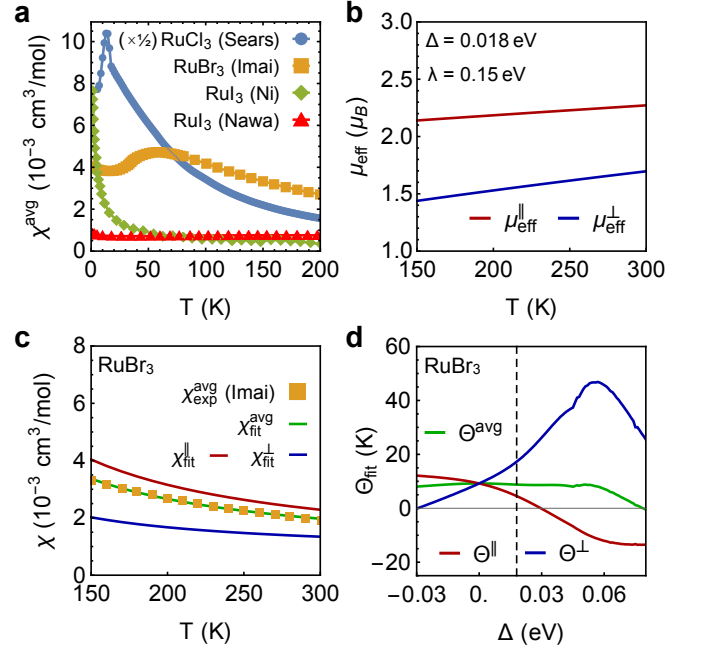


FIG. 2. **Magnetic susceptibility and modified Curie-Weiss fit.** **a** Experimental direction-averaged RuX₃ susceptibility data, extracted from plots in the following references and labelled by respective first-author names: RuCl₃ (Sears) [29], RuBr₃ (Imai) [22], RuI₃ (Ni) [23], RuI₃ (Nawa) [24]. Note that the RuCl₃ curve is scaled by $1/2$. **b** Calculated temperature-dependent effective moment $\mu_{\text{eff}}(T)$ for $\Delta = 0.018 \text{ eV}$ and SOC $\lambda = 0.15 \text{ eV}$. **c** Modified Curie-Weiss fit of RuBr₃ data, taking into account such $\mu_{\text{eff}}(T)$. **d** Dependence of best-fit Weiss constants on assumed Δ . Vertical dashed line indicates $\Delta = 0.018$.

dependent van-Vleck contributions can arise, which can be effectively captured in a temperature-dependent magnetic moment $\mu_{\text{eff}}(T, \Delta)$ [30], as shown for $\Delta = 0.018 \text{ eV}$ in Fig. 2b, where Δ can be directly associated to the crystal field splitting resulting from the distorted octahedral environment of Ru. In fact, for the sister compound RuCl₃, a standard CW fit would lead to $\Theta_{\text{std}}^{\text{avg}} = -20 \text{ K}$, whereas an improved CW fit taking into account such *van-Vleck*-like contributions [30] provides CW constants $\Theta^{\parallel} = +55 \text{ K}$ for the magnetic field in the honeycomb plane and $\Theta^{\perp} = +33 \text{ K}$ for the out-of-plane field, revealing an average CW constant, $\Theta^{\text{avg}} = \frac{2\Theta^{\parallel} + \Theta^{\perp}}{3}$, of $\approx 48 \text{ K}$. This indicates predominant ferromagnetic (FM) interactions, as they have become established for the magnetic Hamiltonian in RuCl₃ [31–34].

Considering a similar strategy (see “Methods” section), we fit the average susceptibility χ^{avg} of RuBr₃ [22]. However, since the crystal-field parameter Δ primarily controls the in-plane vs out-of-plane anisotropy, and for RuBr₃ only powder-averaged data are available, we do not aim at extracting Δ by fitting. Instead, we first fix Δ using our first-principles calculations, enforcing $\mu_{\text{eff}}^{\parallel}/\mu_{\text{eff}}^{\perp}(T = 0 \text{ K}) \propto g_{\parallel}/g_{\perp}$, where g_{\parallel}/g_{\perp} are taken from quantum chemistry

calculations (see Fig. 5a, discussed below). This leads to $\Delta = 0.018$ eV. The best CW fit accounting for the implied $\mu_{\text{eff}}(T, \Delta = 0.018$ eV) (shown in Fig. 2c) yields Weiss constants $\Theta^{\parallel} \approx 5$ K, $\Theta^{\perp} \approx 17$ K and $\Theta^{\text{avg}} \approx 9$ K, which are positive, indicating predominately ferromagnetic interactions for RuBr₃, as seen before in RuCl₃. In Fig. 2d we further analyze how the best-fit Weiss constants evolve for other choices of Δ . Indeed, for a wide range of reasonable Δ around the first-principles value (indicated by the dashed vertical line), the average Weiss constant Θ^{avg} remains positive.

Importantly, for both materials, a standard residual “background” term has to be included in the fitting, which in our case, depending on the material (RuBr₃ or RuCl₃) ranges from $\sim -3.5 \times 10^{-4}$ emu/mol to 1.5×10^{-4} . This is of the same order of magnitude as the corresponding term in RuI₃ (~ 3 to 8×10^{-4} emu/mol). Since in the former cases an intrinsic Pauli origin can be excluded, this observation also casts doubts on a metallic interpretation of this term in RuI₃. Actually, the two available susceptibility measurements on RuI₃ display different behaviors, one nearly temperature-independent [24], and the other [23] showing a Curie-like rise at low temperatures, where a standard CW fit yields $\mu_{\text{eff}} = 0.53\mu_{\text{B}}$ and $\Theta_{\text{CW}}^{\text{avg}} = -3$ K [23]. These differences are consistent with our hypothesis that the measured samples consist of magnetic insulating grains with metallic boundaries in between. Then, the samples with larger resistivity data [23] hint to larger insulating grains, hence less metallic boundaries are present, leading to the low-temperature Curie-like upturn in the susceptibility, compared to the samples in [24].

Electronic and magnetic calculations

In the following we present a comparison of the electronic and magnetic properties of the trihalide RuX₃ family obtained from a combination of density functional theory (DFT) and exact diagonalization of *ab-initio*-derived low-energy models. Details of the calculations are given in the “Methods” section.

Past experience with first-principles calculations for the Ru-based trihalides [5, 35–38] indicates that the magnetic order and, to a considerably lesser extent, metallicity is very fragile, with several closely competing different magnetic phases. The ground states may vary depending on small changes in the crystal structure, on the way in which strong correlations are accounted for, and even on tiny details of the computational protocol. With this in mind, it is imperative to compare the calculated properties across the series, using the exact same computational setup.

For the electronic structure calculations we consider the experimentally reported C2/m [5, 6] and R $\bar{3}$ [39] structures for RuCl₃, and the suggested R $\bar{3}$ structures for RuBr₃ [22] and RuI₃ [23]. Structural details of the four models are

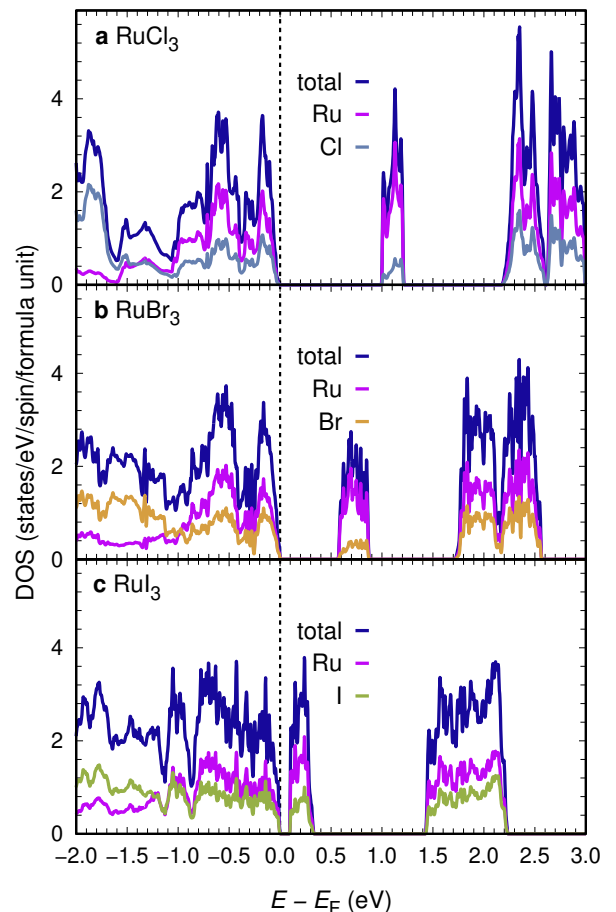


FIG. 3. **Density of states for RuX₃ (X=Cl, Br, I)** Density of states (DOS) for the experimental structures of RuCl₃, RuBr₃ and RuI₃, obtained from GGA+SO+U calculations with Wien2k, considering antiferromagnetic zigzag magnetic configurations. For RuCl₃ we employed $U_{\text{eff}} = 2.7$ eV, for RuBr₃ $U_{\text{eff}} = 2.1$ eV and for RuI₃ $U_{\text{eff}} = 1.4$ eV. Shown is also the contribution of Ru and halogen states to the DOS.

summarized in the Supplementary Information. For RuCl₃, the R $\bar{3}$ results are shown in Supplementary Information due to very similar results to the C2/m ones.

Figure 3 shows the relativistic density of states (DOS) obtained within GGA+SOC+U as implemented in Wien2k, where a zigzag magnetic configuration with magnetic moments polarized perpendicular to the *ab* plane was considered. For the choice of $U_{\text{eff}} = U - J$ we take as a reference the *ab initio* estimates for the orbitally-averaged Hubbard on-site (U_{avg}) and Hund’s coupling (J_{avg}) as obtained from constrained random-phase approximation (cRPA) calculations (see “Methods” section for calculation details). In contrast to previous cRPA estimates for RuCl₃ [40], our estimates incorporate all five *d* orbitals and extend to the complete Ru-based trihalide family. As shown in Fig. 4a, the effective Hubbard interaction parameters decrease with

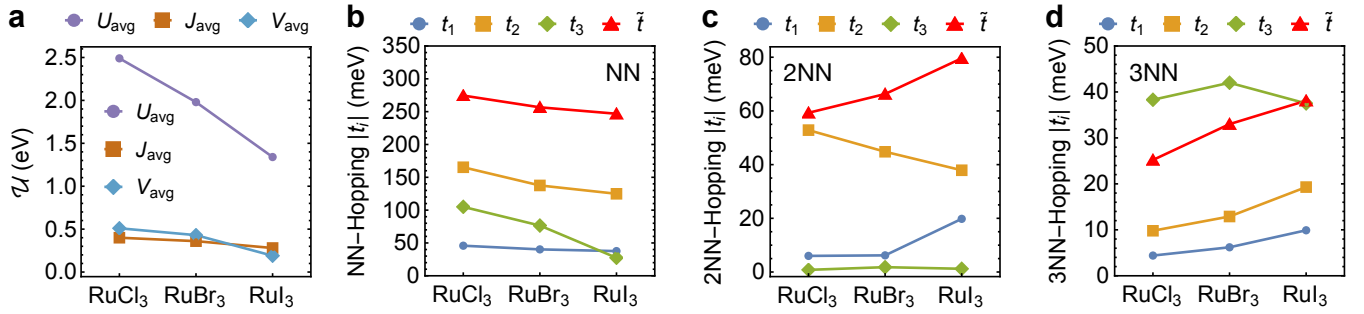


FIG. 4. **Ab-initio-computed multi-orbital Hubbard model parameters across the RuX₃ family.** **a** cRPA results for the orbitally-averaged on-site Hubbard interaction (U_{avg}), Hund's coupling (J_{avg}), and the nearest-neighbour V_{avg} coupling. **b** Absolute magnitude of hopping parameters $t_1 = t_{(yz,yz)}$, $t_2 = t_{(xz,yz)}$, $t_3 = t_{(xy,xy)}$, and $\tilde{t} = t_{(xy,z^2)}$ on nearest-neighbor (NN), second-neighbor (2NN) and third-neighbor (3NN) Z-bonds.

increasing ligand atomic number from Cl to I, which can be attributed to the more delocalized nature of the Ru d orbitals in RuI₃ compared to RuCl₃ when hybridizing with I instead of Cl.

For RuCl₃ a $U_{\text{eff}} = 2.7$ eV yields both the fundamental and direct gap to be ≈ 1 eV (Figure 3a) in agreement with the reported optical gap, apart from the presence of multiplets at 200 meV [41]. We systematically reduced U_{eff} to 2.1 eV for RuBr₃ and 1.4 eV for RuI₃ following the trend given by the cRPA results. With these values, RuBr₃ shows a gap of 0.56 eV, (Figure 3b) while RuI₃ shows a small gap of 0.1 eV (Figure 3c). The gap closes in RuI₃ when U_{eff} is further reduced to 1 eV. These results indicate a spin-orbit assisted Mott insulating state in disorder-free RuI₃ samples, which is on the verge of a metal-insulator transition. Possibly, as discussed above, disorder in the experimental samples could act as effective pressure, and bring the samples closer or over the Mott transition as seen in other Mott insulators [27]. Note that these results hold regardless of the assumed magnetic pattern in the calculations.

In order to analyze the magnetic structure of the RuX₃ compounds, we first consider spin-polarized total energy calculations with VASP in the GGA+SOC+U approximation (see also “Methods”). Detailed results are listed in the Supplementary Information. For RuCl₃, the calculated energy of the ferromagnetic state E_{FM} is very competitive with the energy of the experimentally observed zigzag ordered state E_{ZZ} : $E_{\text{ZZ}} - E_{\text{FM}} \approx 2$ meV/Ru. This observation is consistent with the evidence for a metastable ferromagnetic state in RuCl₃ [34, 42]. Correspondingly, in our effective pseudospin model of RuCl₃ discussed below, the *classical* energy of the ferromagnet is below that of a zigzag, and only by including quantum fluctuations the zigzag ground state is recovered (as in, e.g., Ref. [34]). For RuBr₃ we find an energy minimum for the zigzag ordering in agreement with the experiment. Interestingly, for RuI₃ Néel and zigzag orders are energetically almost degenerate $E_{\text{Néel}} - E_{\text{ZZ}} \approx 1$ meV/Ru, with the rest of magnetic orders we scanned being energetically

rather close. All orders show very small and varying magnetic moments for Ru. These results hint to a magnetic frustration.

We proceed with the derivation of magnetic exchange models. In the first place, the magnetic Hamiltonian of RuBr₃ has been suggested to be closer to the pure Kitaev limit than in RuCl₃ [22], and, secondly, with our proposed scenario of a Mott insulating state for RuI₃, the question of its magnetic properties is open. To investigate these issues from first principles, we derive via the *ab-initio* projED method [43] the pseudospin models $\mathcal{H}_{\text{eff}} = \sum_{ij} \mathbf{S}_i \cdot \mathbb{J}_{ij} \cdot \mathbf{S}_j$ of the three RuX₃ compounds. Here, \mathbf{S} stands for the relativistic pseudospin $j_{\text{eff}} = 1/2$ moment [2].

In the conventional parametrization of Kitaev materials, the exchange matrix \mathbb{J}_{ij} in $R\bar{3}$ symmetry on a nearest-neighbor Z₁-bond (defined in Fig. 1) follows the form

$$\mathbb{J}_{ij} = \begin{pmatrix} J_1 + \nu_1 & \Gamma_1 & \Gamma'_1 + \eta_1 \\ \Gamma_1 & J_1 - \nu_1 & \Gamma'_1 - \eta_1 \\ \Gamma'_1 + \eta_1 & \Gamma'_1 - \eta_1 & J_1 + K_1 \end{pmatrix}, \quad (1)$$

with the isotropic Heisenberg exchange J_1 , the bond-dependent anisotropic Kitaev exchange K_1 , the bond-dependent off-diagonal exchange terms Γ_1 and Γ'_1 and correction terms η_1 and ν_1 . The latter correction terms are found to be small in our calculated Hamiltonians, and are neglected in what follows. The exchange matrices on X- and Y-bonds follow by respective C_3 rotations about the out-of-plane axis ([111] in pseudospin coordinates). Analogously follow the definitions for second and third neighbor exchange terms (or see, e.g., Ref. [4]).

Using U_{avg} and J_{avg} from cRPA (Fig. 4a), the relativistic hopping parameters extracted from DFT (magnitudes shown in Fig. 4b,c,d) and the projED method, we extracted the exchange constants shown in Fig. 5b,c,d.

Evaluating the magnetic interactions of the complete RuX₃ family, we find a nearest-neighbor ferromagnetic Kitaev interaction K_1 to be the dominant in all three compounds. Additionally, a subdominant ferromagnetic nearest-neighbor

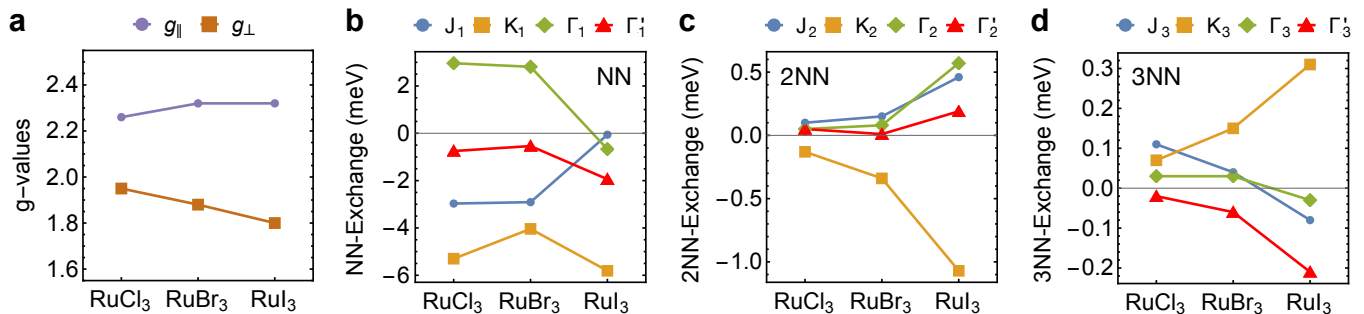


FIG. 5. **Ab-initio computed pseudospin models across the RuX₃ family.** **a** Quantum chemistry results for local gyromagnetic g -tensor components g_{\parallel} (in-plane) and g_{\perp} (out-of-plane). **b-d** projED results for the magnetic exchange couplings on nearest-neighbor (NN), second-neighbor (2NN) and third-neighbor (3NN) bonds. Tabular form of all values is given in Supplementary Information.

Heisenberg exchange J_1 is present, which is, however, almost vanishing for the iodine case. The symmetric off-diagonal Γ_1 interaction is of similar magnitude as J_1 , changing sign going from Cl and Br to I. Γ'_1 , often neglected in the RuCl₃ analysis, may become rather important, particularly for RuI₃. Further-neighbor interactions are generally smaller than their nearest-neighbor counterparts for all three systems, but increase for larger ligand atomic number and may play, especially in RuI₃, an important role.

That the anisotropic interactions do not monotonically increase with stronger spin-orbit coupling of halogen elements can be related to the SOC source. In the original Jackeli-Khaliullin mechanism [2], the heavy magnetic ions are solely responsible for SOC effects, which can be well described within the SOC atomic limit. In the case of RuBr₃ and RuI₃, however, ligand SOC starts to play an important role. To evaluate the interplay of these two SOC sources, we extracted *ab initio* values for the RuX₃ materials and compared them to the SOC atomic limit (see Supplementary Information). We find that in these compounds SOC effects from magnetic ions and ligands do not enhance each other, but do compete. This leads to the observed inhomogeneous behavior of the magnetic anisotropic terms in Fig. 5 as a function of ligand atomic number. Another consequence of this breakdown of the SOC atomic limit is that the established analytic perturbation theory expressions [2–4] become unjustified in Kitaev materials where SOC arises from both the metal and the ligand elements. RuBr₃ and RuI₃ are therefore cases where more general approaches are indispensable, as for example recently derived for the $S = 3/2$ material CrI₃ [44].

Along the halogen series Cl-Br-I we observe a decrease for nearest-neighbor couplings (Fig. 5b) and an overall increase in magnitude for second and third neighbors (Fig. 5c,d). This can be understood by consideration of the ligand-metal (p - d) hybridization. We quantify the hybridization strength by integrating the DFT(GGA) density of states (DOS) with Ru 4d orbital character in the energy window dominated by

the ligand p orbitals (between -7 eV and -1.05 eV). In spite of respective larger Ru-Ru distances, this can be related to the magnetic exchange by consideration of the *ab initio* hopping parameters between Wannier d orbitals. For stronger hybridization the nearest-neighbor hopping parameters are reduced for heavier ligands, illustrated in Fig. 4b. This is reflected in the magnetic exchange parameters (Fig. 5b) in an overall reduced magnitude in the nearest-neighbor parameters. In contrast, the second and third neighbors show a very different dependence on the halogen element. From the dominant further-neighbor hoppings (Fig. 4c,d), the hoppings show an overall tendency to increase, with few exceptions. Certain further-neighbor magnetic exchange parameters, depending on their relation to the individual hopping parameters, become therefore increasingly important for RuBr₃ and especially for the magnetic properties of RuI₃. Finally, we also computed the gyromagnetic g -tensor for the RuX₃ family from first principles, in order to relate the pseudospin \mathbf{S} of the effective Hamiltonian to the magnetic moment $\mathbf{M} = \mu_B \mathbb{G} \cdot \mathbf{S}$. The g -tensor can be approximately characterized by two components, the value parallel to the honeycomb plane, g_{\parallel} , and the one perpendicular to it, g_{\perp} , which are shown in Fig. 5a. We consistently find $g_{\parallel} > g_{\perp}$ for the whole family, promoting a stronger Zeeman term for in-plane fields.

We now discuss the ramifications of the derived magnetic models for the magnetism in these materials.

For RuCl₃, we can compare our result to a vast available literature of models that have been shown to reproduce various experimental observations. Indeed, the model presented here in Fig. 5, derived completely from first principles without adjustments or external parameters, is remarkably close to some well-benchmarked recent models [16, 34, 36], and is therefore expected to also describe the material quite well. As we apply the same *ab-initio* setup for the new members of the RuX₃ family, we expect our models to be reliable for them too.

The direction-averaged Weiss constant ($\Theta_{\text{CW}}^{\text{avg}}$ in Table II) is

RuX ₃	RuCl ₃	RuBr ₃	RuI ₃
Θ_{CW}^{avg}	+39.1 K	+35.6 K	+15.4 K
GS	Zigzag	Zigzag	QSL?
ϕ_M	90°	90°	
θ_M	34.4°	32.4°	

TABLE II. **Properties of derived pseudospin models.** Θ_{CW}^{avg} is the powder-averaged Weiss temperature of each model. “GS” refers to the ground state computed by exact diagonalization, and the angles of the magnetic moment ϕ_M, θ_M are defined according to Fig. 1b.

predicted to be positive across the RuX₃ family, characteristic of *ferromagnetic* exchange interactions. This is in line with our analysis of the experimental magnetic susceptibilities of RuCl₃ and RuBr₃ above (Fig. 2). While in RuCl₃ and RuBr₃ a large FM contribution to the Weiss constant comes from a significant FM nearest-neighbor Heisenberg interaction J_1 , this interaction nearly vanishes for RuI₃ (Fig. 5b), leading to a smaller Weiss constant. Furthermore, the small J_1 in RuI₃ renders the nearest-neighbor interactions to be extremely anisotropic, with a dominant Kitaev interaction K_1 . While at first glance this might suggest a spin-liquid ground state in RuI₃, the increased strength of the further-neighbor interactions in RuI₃ (see, e.g., J_2, K_2 in Fig. 5c) also needs to be considered [45].

To find the magnetic ground state properties, we perform exact diagonalization (ED) calculations of the derived $j_{eff} = 1/2$ models on the 24-site cluster shown in Fig. 6a. In Table II and Fig. 6b we summarize the encountered ground states, i.e. zigzag for RuCl₃ and RuBr₃, but possibly a quantum spin liquid (QSL) in RuI₃. This is discussed in detail below.

For RuCl₃, the model in Fig. 5 (as well as the $R\bar{3}$ model discussed in the Supplementary Information) yields zigzag AFM order, identifiable by a maximum at $\mathbf{k} = \mathbf{M}$ in the static spin structure factor, shown in Fig. 6b. The computed ordered magnetic moment direction (see “Methods” section), parametrized by θ and ϕ in Table II (compare Fig. 1b), is found to be tilted by $\theta_M \approx 34^\circ$ out of the plane, in excellent agreement with the recent experiment, where $\theta_M = 32 \pm 3^\circ$ [33] was reported. Interestingly, on the classical level, the ferromagnetic state is lower in energy than the zigzag state, meaning that the latter only becomes the ground state through quantum fluctuations, as discussed also in Ref. [34].

We will now focus on the recently synthesized compounds, starting with RuBr₃. The static spin structure factor for the RuBr₃ model of Fig. 5 is shown in Fig. 6b, indicating also a zigzag AFM order ($\mathbf{Q} = \mathbf{M}$ and C_6 -rotated vectors), in agreement with experiment [22]. However, the calculated tilt angle of the magnetic moment, $\theta_M = 32^\circ$, is more in line with RuCl₃ than with the reported measured

$\theta_M = 64^\circ$ of RuBr₃ [22]. The authors of Ref. [22] argued that this anomalously large tilt angle indicates an exceptionally strong relative Kitaev coupling, i.e., larger $|K_1/J_1|$ and $|K_1/\Gamma_1|$ compared to RuCl₃. To investigate to what extent a closer proximity to the pure Kitaev model could produce such high tilt angles, we take our RuBr₃ Hamiltonian of Fig. 5 as a starting point and tune towards the pure Kitaev model, where K_1 is the only non-zero coupling. This is done by multiplying every exchange coupling except K_1 by $(1-f)$ and sweeping f from 0 to 1. As shown in Fig. 6c, the moment indeed rotates further away from the honeycomb plane upon moving towards the pure Kitaev model, however even right before the transition to the Kitaev spin liquid (indicated by the vertical dashed line), θ_S does not exceed 46° . $\theta_M = \arccos\left(\frac{\cos\theta_S}{\sqrt{g_{||}^2 \cos^2\theta_S + g_{\perp}^2 \sin^2\theta_S}}\right)$, which is to be compared to the neutron diffraction experiment, is even smaller due to the anisotropy $g_{||} > g_{\perp}$ in our calculated g -tensor (Fig. 5a). A reconciliation with the reported $\theta_M = 64^\circ$ would therefore require quite drastic changes to the g -tensor anisotropy and/or the exchange parameters. While in the whole J_1 - K_1 - Γ_1 parameter space with $\Gamma_1 > 0$, no angles of θ_S beyond $\sim 40^\circ$ are expected in the zigzag phase [46], significant *negative* $\Gamma_1 < 0$ can in principle lead to θ_S beyond 60° [47]. However such terms seem incompatible with the *ab-initio* results and would likely need strong distortions [48] from the present considered RuBr₃ crystal structure to be realized.

More distinct from the other two compounds are our results for RuI₃. As discussed above, in our GGA+SOC+U calculations we find a very flat energy landscape of competitive magnetic configurations, indicative of strong magnetic frustration. Fittingly, the ground state from exact diagonalization of the present exchange model does not show a dominant ordering wave vector in the spin structure factor, see Fig. 6b. Although this is a signature generally associated with quantum spin liquid (QSL) states, we note that in the present model, the Kitaev \mathbb{Z}_2 flux operator yields $\langle W_p \rangle = 2^6 \langle S_1^x S_2^y S_3^z S_4^x S_5^y S_6^z \rangle \approx 0.29$ (site indices refer to Fig. 6a). While this is clearly elevated compared to classical collinear states, where $\langle W_p \rangle$ is restricted to $|\langle W_p \rangle| \leq \frac{1}{27} < 0.04$, it is still significantly below the value of the pure unperturbed Kitaev spin liquid, where $\langle W_p \rangle = 1$ [1]. Hence, if the ground state constitutes a QSL state, it is presumably not the \mathbb{Z}_2 Kitaev spin liquid. The precise nature of the encountered magnetically disordered state might be interesting for future studies. It appears to be stabilized by the further-neighbor interactions, as we find a clear ferromagnetic ground state when omitting the second- and third-neighbor interactions in the present model. While a QSL scenario for our full RuI₃ model is compelling, we note that finite-size effects in our calculation could play a role.

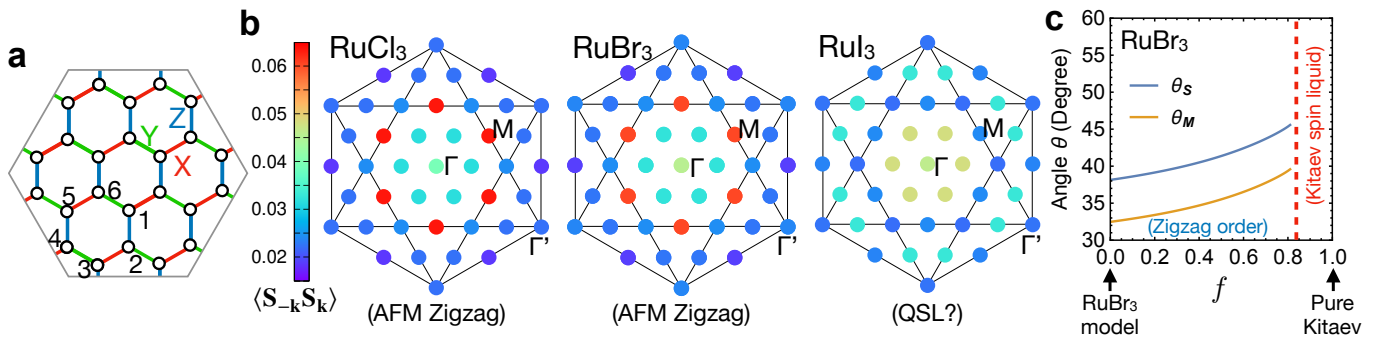


FIG. 6. **Exact diagonalization of RuX_3 pseudospin models.** **a** Employed periodic cluster. Labeled sites 1, \dots , 6 define the Kitaev plaquette operator $W_p = 2^6 S_1^x S_2^y S_3^z S_4^x S_5^y S_6^z$. **b** Static spin structure factor in reciprocal space. Inner (outer) hexagon mark the edge of the first (third) Brillouin Zone. High-symmetry k -points Γ, M, Γ' are labelled. Color scale is the same for all three plots. **c** Out-of-plane angle θ_S (θ_M) of the pseudospin (magnetic moment) within the zigzag phase when tuning from the RuBr_3 model ($f = 0$) towards the pure Kitaev model ($f = 1$). Dashed vertical line indicates phase transition to the Kitaev spin liquid, identified by a peak in $-\partial^2 E / \partial f^2$.

Conclusions and outlook

To summarize, we have presented a comparative analysis of the electronic and magnetic properties of the Ru-based trihalide family, including the recently synthesized RuBr_3 and RuI_3 , by combining state-of-the-art *ab initio* microscopic modelling with analysis of reported resistivity, specific heat and magnetic susceptibility data. The evolution of the magnetic order and Mott-Hubbard correlations along the halogen series, as well as possible role of disorder, have been a central part of our study. We conclude that:

1. All three ideal compounds are spin-orbit-assisted Mott insulators, but their fundamental gap decreases with higher ligand atomic number, $\text{Cl} \rightarrow \text{Br} \rightarrow \text{I}$, with RuI_3 coming rather close to a metal-insulator transition.
2. From DFT total-energy calculations, in ideal, pristine crystals the zigzag magnetic order is even more stable in RuBr_3 than in RuCl_3 , while RuI_3 shows significant magnetic frustration. Our *ab-initio* extracted low-energy models predict RuI_3 to be a quantum spin liquid candidate, which, interestingly, is possibly of a different kind to the \mathbb{Z}_2 Kitaev spin liquid.
3. A number of reported experimental observations seem to be adversely affected by the sample quality, in particular by dirty grain boundaries. In fact, most of the observations in RuI_3 can be reconciled with the theory by assuming insulating grains with (bad) metallic boundaries. The experimental evidence is consistent with a “dirty” insulator, or a bad metal. Disorder would favor either of these.
4. In all three systems the dominant nearest-neighbor interaction is FM Kitaev K_1 , with a subdominant FM Heisenberg Interaction J_1 , that nearly vanishes for RuI_3 . We observe a non-monotonous behavior of

the magnetic anisotropic terms as a function of ligand atomic number that we trace back to a competition of the SOC effects from magnetic ions and ligands.

5. RuBr_3 has predominantly *ferromagnetic* interactions, in contrast to what is suggested by standard Curie-Weiss analysis [22]. Such interactions are consistent with the experimental susceptibility when taking into account high-temperature SOC effects. Our *ab-initio* magnetic model predicts zigzag order in agreement with experiment, with a tilting angle of $\theta_M = 32^\circ$ for the magnetic moments, similar to RuCl_3 , but in contradiction to the reported $\theta_M = 64^\circ$ [22]. We showed that such a large angle cannot be simply explained by proximity to the pure Kitaev model, but would require quite drastic changes to the exchange parameters, such as sizeable negative $\Gamma_1 < 0$. Those would necessitate strong distortions on the reported RuBr_3 crystal structures.

Answering the question posed in the title, our results and analysis strongly suggest that the ideal RuCl_3 , RuBr_3 and RuI_3 compounds constitute a family of three Mott-insulating *siblings*. The challenging task of getting better samples will hopefully help resolve the open issues.

METHODS

Modified Curie-Weiss fit of RuBr_3

We fit the experimental average susceptibility of Ref. [22] with four fitting parameters $\chi_0^\perp, \chi_0^\parallel, \Theta^\perp, \Theta^\parallel$ using the modified Curie-Weiss formula

$$\chi^{\text{avg}}(T) \approx \frac{2}{3} \left(\chi_0^\parallel + \frac{C^\parallel(T)}{T - \Theta^\parallel} \right) + \frac{1}{3} \left(\chi_0^\perp + \frac{C^\perp(T)}{T - \Theta^\perp} \right), \quad (2)$$

where Θ^{\parallel} , Θ^{\perp} are the Weiss constants and $C^{\alpha}(T) \propto [\mu_{\text{eff}}^{\alpha}(T, \Delta)]^2$ is determined through Δ as described in Ref. [30]. Superscripts \parallel and \perp indicate the in- and out-of-honeycomb-plane direction respectively. The susceptibility is fitted over the temperature range 150 – 300 K and SOC strength $\lambda = 0.15$ eV is taken.

DFT calculations

To make sure that the calculated features within density functional theory are robust with respect to the choice of the basis set, we have tested the results using three different methods: the projector augmented wave method [49, 50] as implemented in the VASP code [51, 52], the full potential linearized augmented plane-wave (LAPW) basis as implemented in Wien2k [53] and the full potential local orbital basis set (FPLO) [54]. Throughout the paper we have used the Generalized Gradient Approximation (GGA [55]) to the exchange-correlation functional. Hubbard correlation effects were included on a mean field level in the rotationally invariant implementation of the GGA+U method [56]. All calculations included spin-orbit coupling (SOC) effects. For VASP we used the Ru_pv pseudopotential, treating Ru p states as valence, and the standard pseudopotentials for the halogens. The Γ -centered $8 \times 8 \times 8$ mesh in the nonmagnetic rhombohedral Brillouin zone was used, or the correspondingly scaled meshes for other structures. The energy cut-off was 350 eV, and the energy convergence criterion 1×10^{-08} eV. For each type of magnetic order a number of collinear starting configurations with randomly selected Néel vectors were used, and the lowest-energy result was selected as the ground state. Individual results can be found in the Supplementary Information. For Wien2k we chose the plane-wave cutoff K_{max} corresponding to $RK_{\text{max}} = 8$ and a \mathbf{k} mesh of $8 \times 8 \times 2$ for the $R\bar{3}$ structure in the hexagonal Brillouin zone and $8 \times 4 \times 6$ in the first Brillouin zone of the conventional unit cell for the $C/2m$ structure. The density of states are calculated using a \mathbf{k} mesh of $12 \times 12 \times 3$ for the $R\bar{3}$ structure and $12 \times 6 \times 9$ for the $C/2m$ structure. The zigzag configurations are constructed using a conventional cell of the $C/2m$ structure for RuCl_3 while a $1 \times 2 \times 1$ supercell of the $R\bar{3}$ structures for RuBr_3 and RuCl_3 .

cRPA calculations

In order to obtain *ab-initio* estimates for the effective Coulomb interaction for the Ru-trihalide family, we employed the constrained random-phase approximation (cRPA) [57, 58], as implemented in the FHI-gap code [59], based on the Wien2K electronic structure. The low-energy limit of the screened interaction was projected on the five Ru d orbitals, where screening processes in the same window were excluded. Convergence with respect to the discretization of the Brillouin zone and energy cutoff was ensured.

DFT-based derivation of magnetic models

To derive bilinear exchange parameters for each material, we employed the projED method [43], which consists of two steps. First, complex *ab-initio* hopping parameters between the ruthenium ions are estimated with projective Wannier functions [60] applied on full relativistic FPLO calculations on a $12 \times 12 \times 12$ \mathbf{k} mesh. This allows to construct an effective electronic model $\mathcal{H}_{\text{tot}} = \mathcal{H}_{\text{hop}} + \mathcal{H}_{\text{U}}$, where the complex *ab-initio* hopping parameters enter the kinetic term $\mathcal{H}_{\text{hop}} = \sum_{ij\alpha\beta} \sum_{\sigma\sigma'} t_{i\alpha,j\beta}^{\sigma\sigma'} c_{i\alpha\sigma}^{\dagger} c_{j\beta\sigma'}$ and the cRPA effective Coulomb interaction parameters enter the two-particle term $\mathcal{H}_{\text{U}} = \sum_{i\alpha\beta\gamma\delta} \sum_{\sigma\sigma'} U_{i\alpha\beta\gamma\delta}^{\sigma\sigma'} c_{i\alpha\sigma}^{\dagger} c_{i\beta\sigma'}^{\dagger} c_{i\delta\sigma'} c_{i\gamma\sigma}$. Second, the effective spin Hamiltonian \mathcal{H}_{eff} is extracted from the electronic model via exact diagonalization (ED) and projection of the resulting energy spectrum onto the low-energy subspace, mapped onto pseudo-spin operator representation in the j_{eff} picture with the projection operator \mathbb{P} : $\mathcal{H}_{\text{eff}} = \mathbb{P} \mathcal{H}_{\text{tot}} \mathbb{P} = \sum_{ij} \mathbf{S}_i \mathbb{J}_{ij} \mathbf{S}_j$.

Note that for RuCl_3 the exchange constants slightly differ from previously calculated values by some of the authors [4, 36]. The reason for this lies in the following details of the calculation setup: (i) first principles input parameters U_{avg} and J_{avg} from cRPA in contrast to previous choices, (ii) consideration of all five $4d$ ruthenium orbitals with the cost of restriction onto two-site clusters, (iii) SOC effects considered through complex hopping parameters in contrast to the atomic limit, and (iv) consideration of the experimental crystal structure in contrast to relaxed ambient pressure structure as it was done in Ref. 36.

For the calculation of the gyromagnetic g -tensor, we considered $[\text{RuX}_6]^{3-}$ molecules within the quantum chemistry ORCA 3.03 package [61, 62] with the functional TPSSh, basis set def2-TZVP and complete active space for the d orbitals CAS(5,5).

Exact diagonalization

Exact diagonalization calculations of the $j_{\text{eff}} = 1/2$ models were performed on the 24-site cluster shown in Fig. 6 (a). To identify possible magnetic ordering, we analyze the static spin structure factor $\sum_{\mu=x,y,z} \langle S_{-\mathbf{k}}^{\mu} S_{\mathbf{k}}^{\mu} \rangle$. For the ordered moment direction, we compute the eigenvector with maximal eigenvalue of the correlation matrix $(\langle S_{-\mathbf{k}}^{\mu} S_{\mathbf{k}}^{\nu} \rangle)_{\mu,\nu}$ ($\mu, \nu \in \{x, y, z\}$) at the ordering wave vector $\mathbf{k} = \mathbf{Q}$. This eigenvector then represents the ordered *pseudospin* direction \mathbf{S} [47], which relates to the magnetic moment direction $\mathbf{M} \propto \mathbb{G} \cdot \mathbf{S}$, as measured by neutron diffraction, via the anisotropic g -tensor \mathbb{G} .

Acknowledgments

We thank Stephen M. Winter, Robert J. Cava, Yoshinori Imai, and Elena Gati for discussions and Yoshinori Imai for sharing the structural information of RuBr_3 with us before publication. R.V., A.R., K.R. and D.A.S.K. acknowledge support by the Deutsche Forschungsgemeinschaft (DFG,

German Research Foundation) for funding through Project No. 411289067 (VA117/15-1) and TRR 288 — 422213477 (project A05). Y.L. acknowledges support by National Natural Science Foundation of China (Grant No. 12004296)

and China Postdoctoral Science Foundation (Grant No. 2019M660249). I.I.M. acknowledges support from the U.S. Department of Energy through the grant #DE-SC0021089. R.V. and I.I.M. thank the Wilhelm und Else Heraeus Stiftung for funding.

-
- [1] A. Kitaev, *Ann. Phys.* **321**, 2 (2006).
- [2] G. Jackeli and G. Khaliullin, *Phys. Rev. Lett.* **102**, 017205 (2009).
- [3] J. G. Rau, E. K.-H. Lee, and H.-Y. Kee, *Phys. Rev. Lett.* **112**, 077204 (2014).
- [4] S. M. Winter, Y. Li, H. O. Jeschke, and R. Valentí, *Phys. Rev. B* **93**, 214431 (2016).
- [5] R. D. Johnson, S. C. Williams, A. A. Haghighirad, J. Singleton, V. Zapf, P. Manuel, I. I. Mazin, Y. Li, H. O. Jeschke, R. Valentí, and R. Coldea, *Phys. Rev. B* **92**, 235119 (2015).
- [6] H. B. Cao, A. Banerjee, J.-Q. Yan, C. A. Bridges, M. D. Lumsden, D. G. Mandrus, D. A. Tennant, B. C. Chakoumakos, and S. E. Nagler, *Phys. Rev. B* **93**, 134423 (2016).
- [7] A. Banerjee, J. Yan, J. Knolle, C. A. Bridges, M. B. Stone, M. D. Lumsden, D. G. Mandrus, D. A. Tennant, R. Moessner, and S. E. Nagler, *Science* **356**, 1055 (2017).
- [8] L. J. Sandilands, Y. Tian, K. W. Plumb, Y.-J. Kim, and K. S. Burch, *Phys. Rev. Lett.* **114**, 147201 (2015).
- [9] J. Nasu, J. Knolle, D. L. Kovrizhin, Y. Motome, and R. Moessner, *Nat. Phys.* **12**, 912 (2016).
- [10] S.-H. Do, S.-Y. Park, J. Yoshitake, J. Nasu, Y. Motome, Y. S. Kwon, D. T. Adroja, D. J. Voneshen, K. Kim, T.-H. Jang, J.-H. Park, K.-Y. Choi, and S. Ji, *Nat. Phys.* **13**, 1079 (2017).
- [11] S. Widmann, V. Tsurkan, D. A. Prishchenko, V. G. Mazurenko, A. A. Tsirlin, and A. Loidl, *Physical Review B* **99**, 094415 (2019).
- [12] J. A. Sears, Y. Zhao, Z. Xu, J. W. Lynn, and Y.-J. Kim, *Phys. Rev. B* **95**, 180411 (2017).
- [13] A. Banerjee, P. Lampen-Kelley, J. Knolle, C. Balz, A. A. Aczel, B. Winn, Y. Liu, D. Pajerowski, J. Yan, C. A. Bridges, A. T. Savici, B. C. Chakoumakos, M. D. Lumsden, D. A. Tennant, R. Moessner, D. G. Mandrus, and S. E. Nagler, *npj Quantum Mater.* **3**, 8 (2018).
- [14] Y. Kasahara, T. Ohnishi, Y. Mizukami, O. Tanaka, S. Ma, K. Sugii, N. Kurita, H. Tanaka, J. Nasu, Y. Motome, T. Shibauchi, and Y. Matsuda, *Nature* **559**, 227 (2018).
- [15] R. Hentrich, A. U. B. Wolter, X. Zotos, W. Brenig, D. Nowak, A. Isaeva, T. Doert, A. Banerjee, P. Lampen-Kelley, D. G. Mandrus, S. E. Nagler, J. Sears, Y.-J. Kim, B. Büchner, and C. Hess, *Phys. Rev. Lett.* **120**, 117204 (2018).
- [16] S. M. Winter, K. Riedl, P. A. Maksimov, A. L. Chernyshev, A. Honecker, and R. Valentí, *Nature communications* **8**, 1 (2017).
- [17] R. Hentrich, X. Hong, M. Gillig, F. Caglieris, M. Čulo, M. Shahrokhvand, U. Zeitler, M. Roslova, A. Isaeva, T. Doert, *et al.*, *Physical Review B* **102**, 235155 (2020).
- [18] A. Sahasrabudhe, D. Kaib, S. Reschke, R. German, T. Koethe, J. Buhot, D. Kamenskyi, C. Hickey, P. Becker, V. Tsurkan, *et al.*, *Physical Review B* **101**, 140410 (2020).
- [19] L. E. Chern, E. Z. Zhang, and Y. B. Kim, *Physical Review Letters* **126**, 147201 (2021).
- [20] P. Czajka, T. Gao, M. Hirschberger, P. Lampen-Kelley, A. Banerjee, J. Yan, D. G. Mandrus, S. E. Nagler, and N. Ong, *Nature Physics*, 1 (2021).
- [21] É. Lefrançois, G. Grissonnanche, J. Baglo, P. Lampen-Kelley, J. Yan, C. Balz, D. Mandrus, S. Nagler, S. Kim, Y.-J. Kim, *et al.*, arXiv:2111.05493 (2021).
- [22] Y. Imai, K. Nawa, Y. Shimizu, W. Yamada, H. Fujihara, T. Aoyama, R. Takahashi, D. Okuyama, T. Ohashi, M. Hagihala, S. Torii, D. Morikawa, M. Terauchi, T. Kawamata, M. Kato, H. Gotou, M. Itoh, T. J. Sato, and K. Ohgushi, *Physical Review B* **105**, L041112 (2022).
- [23] D. Ni, X. Gui, K. M. Powderly, and R. J. Cava, *Advanced Materials* **34**, 2106831 (2022).
- [24] K. Nawa, Y. Imai, Y. Yamaji, H. Fujihara, W. Yamada, R. Takahashi, T. Hiraoka, M. Hagihala, S. Torii, T. Aoyama, T. Ohashi, Y. Shimizu, H. Gotou, M. Itoh, K. Ohgushi, and T. J. Sato, *Journal of the Physical Society of Japan* **90**, 123703 (2021).
- [25] R. Jaramillo, S. D. Ha, D. M. Silevitch, and S. Ramanathan, *Nature Physics* **10**, 304 (2014).
- [26] A. Little, L. Wu, P. Lampen-Kelley, A. Banerjee, S. Patankar, D. Rees, C. A. Bridges, J.-Q. Yan, D. Mandrus, S. E. Nagler, and J. Orenstein, *Physical Review Letters* **119**, 227201 (2017).
- [27] E. Gati, U. Tutsch, A. Naji, M. Garst, S. Köhler, H. Schuberth, T. Sasaki, and M. Lang, *Crystals* **8**, 38 (2018).
- [28] O. Tanaka, Y. Mizukami, R. Harasawa, K. Hashimoto, N. Kurita, H. Tanaka, S. Fujimoto, Y. Matsuda, E.-G. Moon, and T. Shibauchi, arXiv:2007.06757 (2020).
- [29] J. A. Sears, M. Songvilay, K. W. Plumb, J. P. Clancy, Y. Qiu, Y. Zhao, D. Parshall, and Y.-J. Kim, *Physical Review B* **91**, 144420 (2015).
- [30] Y. Li, S. M. Winter, D. A. S. Kaib, K. Riedl, and R. Valentí, *Physical Review B* **103**, L220408 (2021).
- [31] S. M. Winter, A. A. Tsirlin, M. Daghofer, J. van den Brink, Y. Singh, P. Gegenwart, and R. Valentí, *Journal of Physics: Condensed Matter* **29**, 493002 (2017).
- [32] P. Laurell and S. Okamoto, *npj Quantum Materials* **5**, 2 (2020).
- [33] J. A. Sears, L. E. Chern, S. Kim, P. J. Bereciartua, S. Francoal, Y. B. Kim, and Y.-J. Kim, *Nature physics* **16**, 837 (2020).
- [34] H. Suzuki, H. Liu, J. Bertinshaw, K. Ueda, H. Kim, S. Laha, D. Weber, Z. Yang, L. Wang, H. Takahashi, *et al.*, *Nature Communications* **12**, 1 (2021).
- [35] H.-S. Kim and H.-Y. Kee, *Physical Review B* **93**, 155143

- (2016).
- [36] D. A. S. Kaib, S. Biswas, K. Riedl, S. M. Winter, and R. Valentí, *Phys. Rev. B* **103**, L140402 (2021).
- [37] H.-S. Kim, arXiv:2111.12291 (2021).
- [38] Y. Zhang, L.-F. Lin, A. Moreo, and E. Dagotto, arXiv:2111.04560 (2021).
- [39] S.-Y. Park, S.-H. Do, K.-Y. Choi, D. Jang, T.-H. Jang, J. Schefer, C.-M. Wu, J. Gardner, J. Park, J.-H. Park, *et al.*, arXiv:1609.05690 (2016).
- [40] C. Eichstaedt, Y. Zhang, P. Laurell, S. Okamoto, A. G. Eguiluz, and T. Berlijn, *Phys. Rev. B* **100**, 075110 (2019).
- [41] L. J. Sandilands, Y. Tian, A. A. Reijnders, H.-S. Kim, K. W. Plumb, Y.-J. Kim, H.-Y. Kee, and K. S. Burch, *Physical Review B* **93**, 075144 (2016).
- [42] S. Bachus, D. A. S. Kaib, Y. Tokiwa, A. Jesche, V. Tsurkan, A. Loidl, S. M. Winter, A. A. Tsirlin, R. Valentí, and P. Gegenwart, *Physical Review Letters* **125**, 097203 (2020).
- [43] K. Riedl, Y. Li, R. Valentí, and S. M. Winter, *Phys. Status Solidi B* **256**, 1800684 (2019).
- [44] P. P. Stavropoulos, X. Liu, and H.-Y. Kee, *Phys. Rev. Research* **3**, 013216 (2021).
- [45] I. Rousochatzakis, J. Reuther, R. Thomale, S. Rachel, and N. B. Perkins, *Physical Review X* **5**, 041035 (2015).
- [46] J. Rusnačko, D. Gotfryd, and J. Chaloupka, *Physical Review B* **99**, 064425 (2019).
- [47] J. Chaloupka and G. Khaliullin, *Physical Review B* **94**, 064435 (2016).
- [48] B. Yang, Y. M. Goh, S. H. Sung, Z. Ye, G. Ye, S. Biswas, D. A. S. Kaib, R. Dhakal, S. Jiang, F. Chen, H. Lei, R. He, R. Valentí, S. M. Winter, R. Hovden, and A. W. Tsien, (2022).
- [49] P. E. Blöchl, *Physical Review B* **50**, 17953 (1994).
- [50] G. Kresse and D. Joubert, *Physical Review B* **59**, 1758 (1999).
- [51] G. Kresse and J. Hafner, *Physical Review B* **47**, 558 (1993).
- [52] G. Kresse and J. Furthmüller, *Computational materials science* **6**, 15 (1996).
- [53] P. Blaha, K. Schwarz, G. K. H. Madsen, D. Kvasnicka, and J. Luitz, WIEN2k, An Augmented Plane Wave Plus Local Orbitals Program for Calculating Crystal Properties (Karlheinz Schwarz, Techn. Universität Wien, Austria) (2001).
- [54] K. Koepnik and H. Eschrig, *Physical Review B* **59**, 1743 (1999).
- [55] J. P. Perdew, K. Burke, and M. Ernzerhof, *Physical Review Letters* **77**, 3865 (1996).
- [56] V. I. Anisimov, I. V. Solovyev, M. A. Korotin, M. T. Czyżyk, and G. A. Sawatzky, *Phys. Rev. B* **48**, 16929 (1993).
- [57] F. Aryasetiawan, M. Imada, A. Georges, G. Kotliar, S. Biermann, and A. I. Lichtenstein, *Phys. Rev. B* **70**, 195104 (2004).
- [58] F. Aryasetiawan, K. Karlsson, O. Jepsen, and U. Schönberger, *Phys. Rev. B* **74**, 125106 (2006).
- [59] H. Jiang, R. I. Gómez-Abal, X. Li, C. Meisenbichler, C. Ambrosch-Draxl, , and M. Scheffler, *Computer Phys. Commun.*,184, 348 **184**, 348 (2012).
- [60] H. Eschrig and K. Koepnik, *Phys. Rev. B* **80**, 104503 (2009).
- [61] F. Neese, *Wiley Interdiscip. Rev. Comput. Mol. Sci.* **2**, 73 (2012).
- [62] F. Neese, *J. Chem. Phys.* **122**, 034107 (2005).